entropy

MDPI

Article

The Relevance of Foreshocks in Earthquake Triggering: A Statistical Study

Eugenio Lippiello [1], Cataldo Godano [1] and Lucilla de Arcangelis [2,*]

[1] Department of Mathematics and Physics, University of Campania "L. Vanvitelli", Viale Lincoln 5, 81100 Caserta, Italy; eugenio.lippiello@unicampania.it (E.L.); cataldo.godano@unicampania.it (C.G.)
[2] Department of Engineering, University of Campania "L. Vanvitelli', Via Roma 29, 81031 Aversa (CE), Italy
* Correspondence: lucilla.dearcangelis@unicampania.it

Received: 25 October 2018; Accepted: 1 February 2019; Published: 13 February 2019

Abstract: An increase of seismic activity is often observed before large earthquakes. Events responsible for this increase are usually named foreshock and their occurrence probably represents the most reliable precursory pattern. Many foreshocks statistical features can be interpreted in terms of the standard mainshock-to-aftershock triggering process and are recovered in the Epidemic Type Aftershock Sequence ETAS model. Here we present a statistical study of instrumental seismic catalogs from four different geographic regions. We focus on some common features of foreshocks in the four catalogs which cannot be reproduced by the ETAS model. In particular we find in instrumental catalogs a significantly larger number of foreshocks than the one predicted by the ETAS model. We show that this foreshock excess cannot be attributed to catalog incompleteness. We therefore propose a generalized formulation of the ETAS model, the ETAFS model, which explicitly includes foreshock occurrence. Statistical features of aftershocks and foreshocks in the ETAFS model are in very good agreement with instrumental results.

Keywords: forecasting; foreshocks; ETAS model

1. Introduction

The epidemic-type-aftershock sequence ETAS model [1–3] is presently considered "a de facto standard model, or null hypotheses, for other models and ideas to be compared to" [4]. The model assumes that two classes of earthquakes exist: Independent background and triggered earthquakes. An epidemic organization of events arises under the assumption that each earthquake can trigger its own descendants leading to a branching organization. From a physical point of view, background seismicity can be thought as the effect of the slow tectonic drive whereas triggered earthquakes are induced by stress redistribution after previous shocks. The interplay between background and triggered seismicity leads to non trivial spatio-temporal patterns which can be highlighted by the complex behavior of the inter-event time distribution [5–9] and are also evident in natural time analysis [10,11] (see ref. [12] for a Review). In the ETAS model the occurrence rate of triggered events is obtained on the basis of well established empirical laws controlling the spatio-temporal clustering of aftershocks. More precisely:

- A1: The number of aftershocks n_a depends on the mainshock magnitude m_M according to the productivity law $n_a = K_a 10^{\alpha_a m_M}$;
- A2: The aftershock number decays as function of the time Δt from the mainshock, consistently with the Omori law $n_a(\Delta t) \sim \Delta t^{-p}$ with $p \simeq 1$;
- A3: The distribution of epicentral distances between mainshock and aftershocks $G(\Delta r, m_M)$ clearly depends on the mainshock magnitude m_M.

These laws are implemented in a branching process where each event can trigger its own aftershocks. By construction, the ETAS model is very efficient in reproducing statistical features (A1–A3) of aftershock organization, observed in instrumental catalogs. At the same time, in the ETAS model an event can trigger also a larger shock. In this situation the triggering event is often named "foreshock" and the triggered earthquake, if it is the largest event in the sequence, is named "mainshock".

In this study, we adopt the standard definition of mainshocks as events sufficiently isolated in time and space from other larger events. Foreshocks (aftershocks) are then all events occurring close in space and in time before (after) the mainshock. We wish to stress that within the ETAS framework, this classification of events does not reflect different physical properties since, as anticipated, only two kinds (independent or triggered) earthquakes are assumed and, for instance, a mainshock can be either an independent or a triggered earthquake. On the other hand, according to a nucleation theory [13–15], the nucleation phase can be characterized by the occurrence of smaller earthquakes inside the region involved in the fracture process of the subsequent incoming larger shock. This pre-shock seismicity is not implemented in the ETAS model and the main question addressed in this study is if its inclusion, within the ETAS modeling, gives a more accurate description of foreshock organization in instrumental catalogs.

In recent years, different studies have enlightened some differences between statistical features of foreshocks in instrumental and in ETAS catalogs [12,16–30]. In this study we will focus on the two main differences:

- F1: The average foreshock number in instrumental catalogs is significantly larger than the one expected according to the ETAS model;
- F2: The organization in space of instrumental foreshocks exhibit a dependence on the mainshock magnitude not predicted by the ETAS model.

In our study, we first investigate whether the incompleteness of instrumental data sets can justify the above differences. We will show that none of the two features can be attributed to spurious incompleteness. This motivates a generalization of the ETAS model, the ETAFS model, which implements the hypothesis that each event can be anticipated by a cluster of smaller earthquakes. This extra ingredient allows us to generate numerical ETAFS catalogs with statistical features of foreshocks in agreement with instrumental catalogs. In the following section we recall the ETAS model and introduce its generalizations considered in this study. Section 3 presents statistical features of foreshocks and aftershocks in instrumental catalogs. In the subsequent section these features are compared with those obtained in numerical catalogs. Conclusions are drawn in the final section.

2. Epidemic Models for Aftershocks and Foreshock Occurrence

2.1. The ETAS Model

The ETAS model is specified by the conditional intensity function, which represents the expected seismicity rate in a given space position conditioned to a given observational history. The conditional intensity function $\Lambda(m, \vec{x}, t)$, which represents the occurrence probability of events with magnitude $m \geq m_c$ in the position $\vec{x}$ at time t, can be written in the following form:

$$\Lambda(m, \vec{r}, t) = \left[\mu w(\vec{r}) + \sum_{i:t_i<t} (|\vec{r}_i - \vec{r}|, t - t_i, m_i) \right] \frac{1}{b \log(10)} 10^{-b(m-m_c)}, \quad (1)$$

where $\mu w(\vec{r})$ is a time independent contribution which reflects the spatial distribution of background seismicity. In the ETAS model one assumes that aftershock occurrence time, epicentral coordinates and magnitude are independent variables and the form of the spatio-temporal kernel $Q(\Delta r_i, t - t_i, m_i)$ is obtained implementing the three well established laws for aftershock triggering (A1–A3) leading to

$$\Lambda_{ETAS}(m,\vec{r},t) = \left[\mu w(\vec{r}) + \frac{A(p-1)}{c}\sum_{i:t_i<t} 10^{\alpha(m_i-m_c)}\left(1+\frac{t-t_i}{c}\right)^{-p} G(\Delta r_i, m_i)\right] \frac{1}{b\log(10)} 10^{-b(m-m_c)}, \quad (2)$$

where $\Delta r_i = |\vec{r}_i - \vec{r}|$ and the sum extends over all events with magnitude m_i, epicentral coordinates $\vec{x}_i$ and occurrence time $t_i < t$. Here, $G(\Delta r_i, m_i)$ is the spatial distribution of aftershock epicentral distances in instrumental catalogs obtained from feature A3.

The first step in the numerical simulation is the generation of the background independent events. To this extent, we initially fix the temporal duration of the catalog T so that $N_m = \mu T$ independent events are randomly located within the temporal interval $[0, T]$. For the spatial position of the background events, we construct a fine space-covering grid of N_c cells and events are located within a cell with probability $w(\vec{r}_i)$ where $\vec{r}_i$ is the position of the cell center. We assign a magnitude $m \geq m_c$ to each event according to the Gutenberg-Richter law $p(m) = \frac{1}{b\log(10)} 10^{-b(m-m_c)}$. The second step is the "first generation" of aftershocks that we obtain associating to each event i, generated at the previous step, several aftershocks $n_a(m_i)$. We extract the value of $n_a(m_i)$ from a Poisson distribution with average $A10^{\alpha(m_i-m_c)}$. The temporal and spatial distance from its mother event of a first-order generation aftershocks is randomly extracted according to features A2 and A3, respectively. More precisely, we obtain occurrence time $\Delta t = t - t_i$ from the Omori-Utsu law (A2) and the epicentral distance Δr_i according to the procedure described in Lippiello et al. [29]. This procedure allows us to implement in numerical simulations the spatial distribution of aftershocks measured in the instrumental catalog. We also assume an isotropic aftershock distribution whereas magnitudes are always assigned according to the Gutenberg-Richter law. Once all first generation aftershocks have been triggered, we iterate the process at the subsequent step in order to determine the second order generation of aftershocks considering as mother event the first order aftershocks. We then iterate the process until no further aftershocks are triggered. A final sorting procedure is applied to reorder all events according to their occurrence time.

2.2. The ETAS Incomplete Catalog

Because of the overlap of seismic coda waves, many aftershocks are not recorded in particular in the first temporal periods after large shocks [31–40]. The direct inspection of seismic signals [37,40] has shown that at a temporal distance τ after an event of magnitude m_0, there exists a lower magnitude level $m_x(\tau, m_0)$ such that it is impossible to detect events with $m \leq m_x(\tau, m_0)$. Results indicate a logarithmic decay of $m_x(\tau, m_0)$ in time

$$m_x(\tau, m_0) = m_0 - \psi \log(\tau) - \Delta m \quad (3)$$

with $\psi \simeq 1$ and $\Delta m \simeq 1$, if τ is measured in seconds. Accordingly, earthquakes can be hidden by larger events preceding them at small temporal distances.

In our study we take explicitly into account the aftershock incompleteness adopting the same procedure developed in [40] to reproduce both the non-trivial dependence of the c-value in the OU law on the mainshock magnitude [8,41–46], as well as the non trivial magnitude correlations between subsequent earthquakes [11,47–53]. The model, defined as ETASI2 model, implements aftershock incompleteness by multiplying the occurrence rate $Q(\Delta r, t - t_i, m_i)$ in Equation (1) by a detection rate function of the magnitude $\Phi(m|q,\sigma)$ represented by the cumulative distribution function of the normal distribution. The function $\Phi(m|q,\sigma)$ depends on two parameters q and σ representing, respectively, the magnitude with a 50% detection rate and a partially detected magnitude range. In other words, $\Phi(q|q,\sigma) = 0.5$ whereas $\Phi(m|q,\sigma) \simeq 0$ when $m < q - \sigma$ and $\Phi(m|q,\sigma) \simeq 1$ when $m > q - \sigma$. In the ETASI2 model the q parameter depends on time according to Equation (3), $q = m_x(\tau, m_i)$.

Numerical ETASI2 catalogs are obtained starting from the complete data set generated via the standard ETAS model. For each couple of events in the ETAS catalog, with magnitudes m_i, m_j and

occurrence times $t_i > t_j$, we evaluate the quantity $q_{ij} = m_x(t_i - t_j, m_j)$ with $m_x(\tau, m_0)$ given in Equation (3). The event t_i, m_i is then removed from the catalog with a probability $\prod_j \left[1 - \Phi(m_i|q_{ij}, \sigma)\right]$ where the product extends over all events with $t_j < t_i$ occurred within a radius of 100 km from the epicenter of the i-th earthquake.

2.3. The ETAFS Model

In this study, we propose a novel model, the Epidemic Type Aftershocks and Foreshock Sequence (ETAFS) model. The model, together with the standard aftershock triggering, assumes that events can be also anticipated by a cluster of smaller events not assumed in the ETAS model. More precisely, in the ETAFS model aftershocks are triggered with the same occurrence probability Λ_{ETAS} of the ETAS model (Equation (2)). The new ingredient is that each earthquake can be also anticipated by several foreshocks leading to

$$\Lambda_{ETAFS}(m, \vec{r}, t) = \Lambda_{ETAS}(m, \vec{r}, t) + \sum_{i:t_i>t}^{ETAS} Q_f\left(|\vec{r}_i - \vec{r}|, t - t_i, m_i\right) \frac{1}{b\log(10)} 10^{-b(m-m_c)}, \tag{4}$$

with

$$Q_f(\Delta r, t - t_i, m_i) = \frac{B(p-1)}{c'} 10^{\alpha'(m_i - m_c)} \left(1 + \frac{t_i - t}{c'}\right)^{-p} G_f(\Delta r_i, m_i), \tag{5}$$

where the sum is restricted to events occurred at time $t_i > t$ according to the first addend in Equation (4) Λ_{ETAS}. We assume that the spatial organization of foreshocks is similar to the aftershock one and then we take $G_f(\Delta r_i, m_i) = G(\Delta r_i, m_i)$ in Equation (2). Moreover we implement an inverse-Omori law with the same p as for aftershock occurrence, to reduce the number of model parameters. This choice has no physical justification for it and we expect that similar results can be recovered with other functional forms of temporal clustering.

The organization in time and space of events triggered according to kernel Q_f in Equation (4), as well as their number, depends on the occurrence time, location and magnitude of the incoming larger event. This violates time causality since the occurrence probability of an event depends on future events. However, from the point of view of point-processes, the model is well defined and the second addend Q_f in Equation (4) can be simply viewed as a further generation step in the branching process. More precisely. The ETAFS catalog is simulated completing all the aftershock generation steps of the ETAS model, according exactly to the procedure outlined in Section 2.1, and assuming a further generation step which correspond to the generation of foreshocks. These are generated with the same rules implemented for aftershocks with the difference that the sign of $\Delta t = t - t_i$ must be subsequently inverted. Magnitudes are again extracted from the Gutenberg-Richter law but with the additional constraint that the foreshock magnitude must be smaller than m_i. We stress that the process of foreshock generation is not iterated: A foreshock does not trigger other aftershocks and is not anticipated by other foreshocks.

Catalog incompleteness can be also taken into account within the ETAFS model by applying the same procedure outlined in Section 2.2 to obtain ETASI2 from ETAS catalogs.

3. Results in the Instrumental Catalogs

3.1. Data Sets and the Definitions of Mainshocks, Aftershocks and Foreshocks

We perform a systematic analysis of four different instrumental catalogs: The relocated Southern California earthquake catalog (RSCEC) [54] (from 01/01/1981 to 12/31/2013), the relocated Northern California earthquake catalog (RNCEC) [55] (from 01/01/1981 to 06/30/2011), the Italian earthquake catalog (ItEC) [56] (from 01/01/2002 to 12/31/2012) and the Japanese earthquake catalog (JaEC) [57] (from 01/01/1966 to 01/30/2011). We use the same definition of mainshock, aftershocks and foreshocks adopted in [29]. More precisely, we define an event as "mainshock" if a larger earthquake does not

occur in the previous y days and within a distance L. In addition a larger earthquake must not occur in the selected area in the following y_2 days. We then associate to each mainshock its own "aftershocks" and "foreshocks" defined as all earthquakes recorded in the subsequent or in the preceding time interval $T = 12$ h, respectively, and within a circle of radius $R \leq R_M$ centered in the mainshock epicenter. We use different R_M for different catalogs: $R_M = 2$ km for RSCEC and RNEC, $R_M = 5$ km for ItEC and $R_M = 10$ km for JaEC.

The choice of parameters has been deeply investigated in previous studies [17,29,50,58] and here we implement typical values, $L = 100$ km, $y = 3$ and $y_2 = 0.5$. The value of R_M is fixed imposing that for each instrumental catalog, different choices of $T \leq 12$ h produces similar results $\rho_a(\Delta r, m_M)$ when $\Delta r < R_M$. This leads to $R_M = 2, 2, 5, 10$ km, for RSCEC, NSCEC; ItEC and JMAC, respectively (see Figure 17 in [29]). We observe that the temporal interval considered for aftershock and foreshock occurrence $[-T, T]$ is always included in the temporal interval $[-y, y_2]$ days, where events larger than the mainshock cannot occur. This choice therefore implies that aftershocks and foreshocks are assumed to be smaller than the mainshock, by definition.

Once mainshocks are identified, they are grouped in classes according to their magnitude $m \in [m_M, m_M + 1)$ and, for each catalog, we evaluate the total number of mainshocks belonging to the given class $n_{main}(m_M)$, the total number of aftershocks $n_{aft}(m_M)$ which follow mainshocks in the given class and the total number of foreshocks $n_{fore}(m_M)$ which anticipate mainshocks in the given class. We also evaluate the epicentral distance Δr between each main-aftershock and main-foreshock couple and construct the aftershock and foreshock epicentral distance distributions, $\rho_a(\Delta r, m_M)$ and $\rho_f(\Delta r, m_M)$.

3.2. The Aftershock and Foreshock Number

In our study, we consider all events with magnitude above a magnitude threshold $m_{th} = 2$. The lower threshold m_{th} must not be confused with m_c in Equation (2). Indeed, m_c is a fixed parameter of the ETAS model and synthetic catalogs contain only events with $m \geq m_c$. The lower magnitude m_{th}, conversely, is a parameter implemented in the data analysis and it can be arbitrarily varied with $m_{th} \geq m_c$.

In Figure 1, we plot the ratio between aftershock and mainshock number $n_{aft}(m_M)/n_{main}(m_M)$ for different mainshock classes m_M and for the different instrumental catalogs. We also plot the ratio between foreshock and mainshock number $n_{fore}(m_M)/n_{main}(m_M)$.

Results in Figure 1 show that the aftershock number is systematically larger than the foreshock number and this difference increases for increasing m_M. The aftershock number is consistent with the Utsu-productivity law (A1)

$$n_{aft}(m_M)/n_{main}(m_M) = K_a 10^{\alpha m_M} \tag{6}$$

and a similar law is also observed for foreshocks $n_{fore}(m_M)/n_{main}(m_M) = K_f 10^{\alpha_f m_M}$.

3.3. Aftershock and Foreshock Spatial Distribution

In Figure 2 we plot, for different catalogs, the average epicentral distance $\zeta_a(\Delta r, m_M)$ defined as as $\zeta_a(\Delta r, m_M) \equiv \frac{1}{\Delta r} \int_0^{\Delta r} d(\Delta r') \Delta r' \rho_a(\Delta r', m_M)$, were $\rho_a(\Delta r, m_M)$ is the aftershock epicentral distribution. We also define the average foreshock epicentral distance

$$\zeta_f(\Delta r, m_M) \equiv \frac{1}{\Delta r} \int_0^{\Delta r} d(\Delta r') \Delta r \rho_f(\Delta r', m_M)$$

where $\rho_f(\Delta r, m_M)$ is the foreshock epicentral distribution.

Figure 2 shows that for all catalogs, data corresponding to different m_M are well separated and in all cases $\zeta_a(\Delta r, m_M) \simeq \zeta_f(\Delta r, m_M)$. The latter result is a direct consequence of the similarity $\rho_a(\Delta r, m_M) \simeq \rho_f(\Delta r, m_M)$ [29].

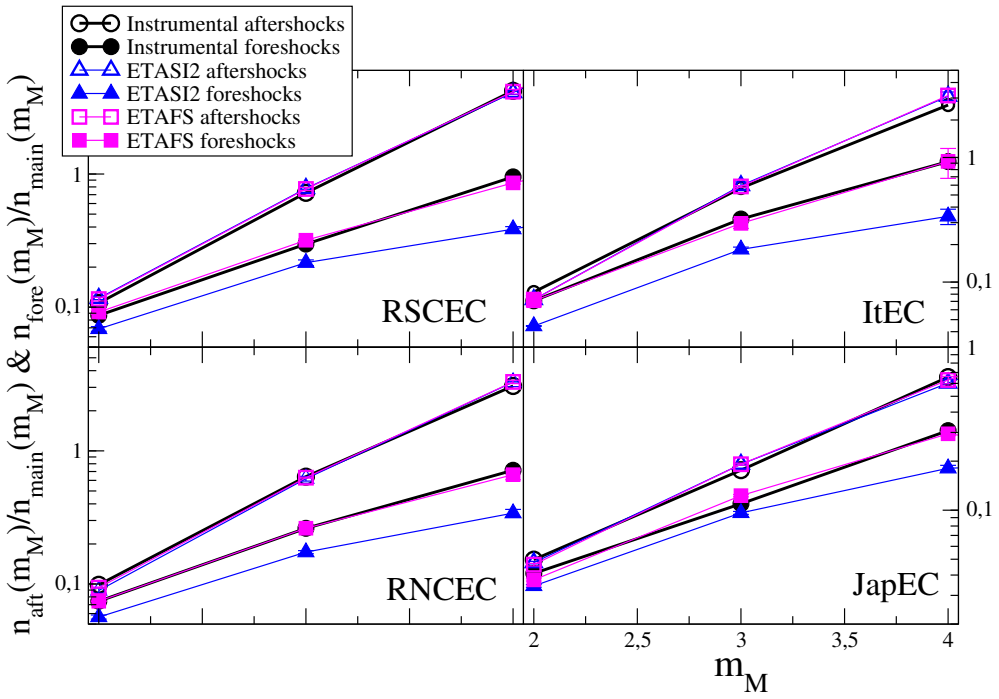

Figure 1. (Color online) The ratio $n_{aft}(m_M)/n_{main}(m_M)$ and $n_{fore}(m_M)/n_{main}(m_M)$ in instrumental and synthetic catalogs. Different panels correspond to different instrumental catalogs. We use open symbols for $n_{aft}(m_M)/n_{main}(m_M)$ and filled symbols for $n_{fore}(m_M)/n_{main}(m_M)$. Results from the instrumental data sets are indicated with black circles. Green triangles are results for the ETASI2 model and red squares for the ETAFS model. The error bars (of the same size of symbols) in numerical catalogs represent the standard deviation from 100 realization of synthetic catalogs. The best parameter of the ETAFS model are listed in Table 1 whereas for the ETASI2 model the best agreement is obtained with $A = 0.084$, $\alpha = 0.9$ and $\mu = 5.85 \times 10^{-4}$ s^{-1} for RSCEC, $A = 0.082$, $\alpha = 0.88$ and $\mu = 4.98 \times 10^{-4}$ s^{-1} for RNCEC, $A = 0.082$, $\alpha = 0.88$ and $\mu = 5.21 \times 10^{-4}$ s^{-1} for ItEC and $A = 0.26$, $\alpha = 0.60$ and $\mu = 5.92 \times 10^{-3}$ s^{-1} for JapEC.

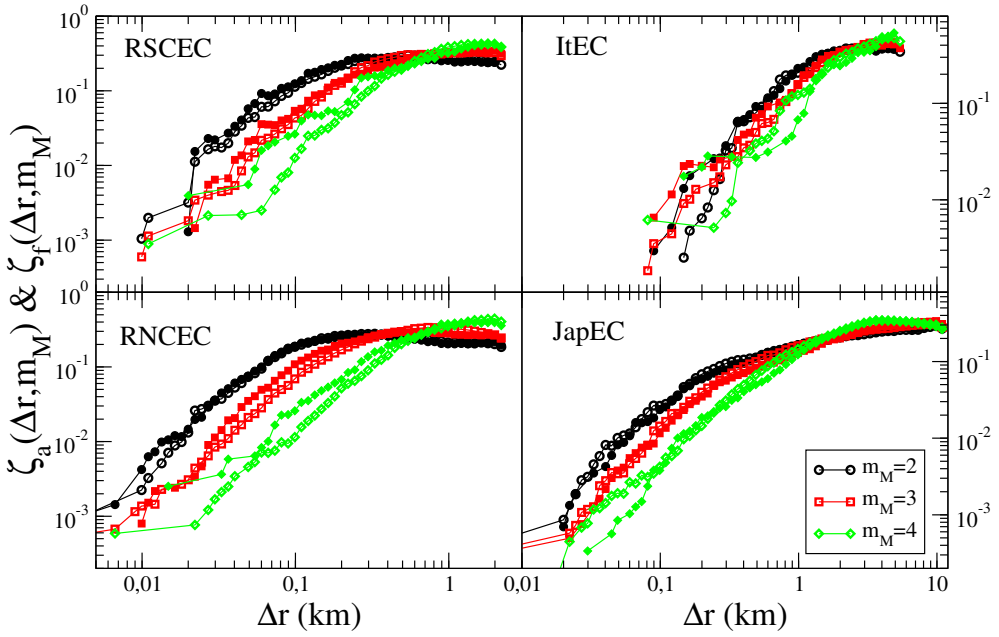

Figure 2. (Color online) The average distance $\zeta_a(\Delta r, m_M)$ of aftershocks (open symbols) and of foreshocks $\zeta_f(\Delta r, m_M)$ (filled symbols) is plotted as function of Δr for the different catalogs. Different mainshock magnitude classes are plotted with different colors and symbols.

4. Results in Numerical Catalogs

4.1. Results in the ETAS Catalog

The Aftershock and Foreshock Number in the ETAS Catalog

In Figure 1, we compare results for $n_{aft}(m_M)/n_{main}(m_M)$ and $n_{fore}(m_M)/n_{main}(m_M)$ with the results obtained applying the same definition of aftershocks, mainshocks and foreshocks to ETAS catalogs. The values of both $n_{aft}(m_M)/n_{main}(m_M)$ and $n_{fore}(m_M)/n_{main}(m_M)$ depend on the parameters A, p, c, α (Equation (2)) of the numerical model. In particular, in first approximation, neglecting the contribution μ of background events from Equation (2) we obtain

$$n_{aft}(m_M) \propto 10^{\alpha(m_M - m_c)} \tag{7}$$

which indicates that the ETAS model can reproduce the experimental result Equation (6) with $\alpha_f = \alpha$.

In numerical simulations we have explored a wide range of ETAS parameters A, p, c, α and verified that there exists a set of parameters leading to ETAS catalogs with the same behavior of $n_{aft}(m_M)/n_{main}(m_M)$ of the instrumental ones. In all cases the agreement between ETAS and instrumental catalogs is always recovered for values of $\alpha \gtrsim \alpha_f$. We wish to stress the difference between α and α_f: α is the model parameter which controls the productivity law in numerical simulations whereas α_f is the value obtained applying our definition of mainshock and aftershock to ETAS catalogs and then performing a fit according to Equation (6). The small discrepancies between α and α_f can be attributed to the background contribution which weakly affects data at small m_M whereas it can be neglected for increasing m_M.

A central observation is that all choices of parameters producing agreement in $n_{aft}(m_M)/n_{main}(m_M)$ between ETAS and instrumental catalogs give a value of $n_{fore}(m_M)/n_{main}(m_M)$ in ETAS catalogs systematically smaller than the instrumental value. It is difficult to obtain a simple approximated expression for the foreshock number as function of m_M as in Equation (7). However, it is reasonable to expect that the ratio $n_{aft}(m_M)/n_{fore}(m_M)$ is mainly controlled by the parameter α and weakly depends on the other model parameters. This is supported by numerical simulations where we fix α in order to have the same value of α_f in ETAS catalogs. Results plotted in Figure 3 show that different choices of A, p, c lead to similar results for $n_{fore}(m_M)/n_{aft}(m_M)$, in all cases, significantly smaller than the experimental value for any m_M.

4.2. Aftershock and Foreshock Spatial Distribution in the ETAS Catalog

The average spatial distribution of aftershocks and foreshocks in ETAS catalogs is plotted in Figure 4. Results show that even if one can generate ETAS catalogs with $\zeta_a(\Delta r, m_M)$ in good agreement with instrumental catalogs (Figure 4a), significant differences are observed between the numeric and the experimental $\zeta_f(\Delta r, m_M)$ (Figure 4b). This difference becomes more pronounced for increasing m_M and can simply attributed to the nature of foreshocks in the ETAS model which are typical events that have triggered a larger shock. Indeed, neglecting the contribution of background seismicity, we indicate by $p(m|m_0)$ the probability that an event with magnitude m_0 triggers an earthquake with magnitude m inside a temporal window T. The epicentral distribution is approximatively given by $\rho(\Delta r, m_0) \simeq p(m|m_0)G(\Delta r, m_0)$. To evaluate the aftershock epicentral distribution $\rho_a(\Delta r, m_M)$ we must restrict to triggered events with $m < m_0$ and integrate over all values of $m_0 \in [m_M, m_M + dM)$,

$$\rho_a(\Delta r, m_M) \simeq \frac{\int_{m_M}^{m_M+dM} dm_0 \int_{m_{th}}^{m_0} dm G(\Delta r, m_0) p(m|m_0)}{\int_{m_M}^{m_M+dM} dm_0 \int_{m_{th}}^{m_0} dm p(m|m_0)}. \tag{8}$$

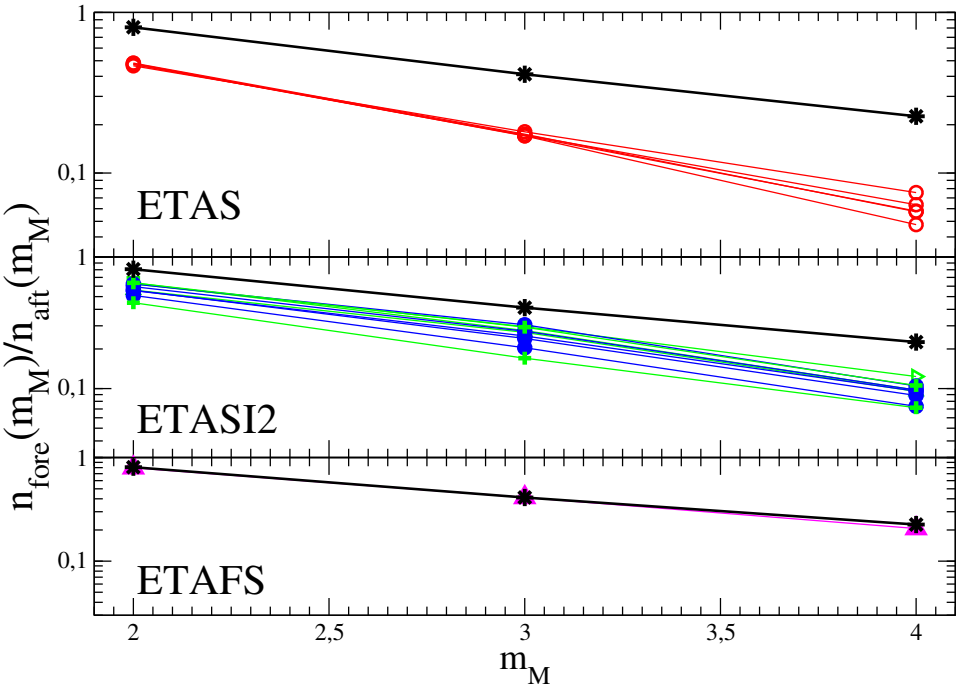

Figure 3. (Color online) The ratio $n_{fore}(m_M)/n_{aft}(m_M)$ in the RSCEC catalog (black stars) is compared with the value obtained in synthetic ETAS (upper panel), ETASI2 (central panel) and ETAFS (lower panel) catalog. (Upper panel) The red open symbols are results for the ETAS model for different choices of the parameters $A \in [0.05, 0.12]$, $p \in [1.1, 1.25]$ and $c \in [0.001, 0.1]$. (Central Panel) The blue filled symbols are results for the ETASI2 model implementing Equation (3) with $\phi = 0.75$ and $\Delta m = 0.8$ and for different choices of the parameters $A \in [0.05, 0.12]$, $p \in [1.1, 1.25]$ and $c \in [0.001, 0.1]$. Green symbols correspond to $A = 0.084$, $c = 0.01$ and $p = 1.2$ used in Figure 1 for the RSCEC catalog and considering different values of ϕ, Δm and σ. (Lower panel) The filled magenta up triangles are results of the ETAFS model with the best set of parameters listed in Table 1.

Conversely, to evaluate $\rho_f(\Delta r, m_M)$ we must consider triggered earthquakes with $m > m_0$ and since m is identified as a mainshock, its magnitude is constrained in the interval $m \in [m_M, m_M + dM)$. Taking into account that the magnitude of the triggering earthquake m_0, identified as a foreshock, is inside the interval $m_0 \in [m_{th}, m)$ we obtain

$$\rho_f(\Delta r, m_M) \simeq \frac{\int_{m_M}^{m_M+dM} dm \int_{m_{th}}^{m} dm_0 G(\Delta r, m_0) p(m|m_0)}{\int_{m_M}^{m_M+dM} dm \int_{m_{th}}^{m} dm_0 p(m|m_0)}. \quad (9)$$

We wish to stress the fundamental difference between Equations (8) and (9) due to the inversion between m and m_0 of the integration range. In Equation (8) the spatial distance is controlled by the kernel $G(\Delta r, m_0)$ which depends on $m_0 \in [m_M, m_M + dM)$ and if $dM \to 0$ $\rho_a(\Delta r, m_M) \simeq G(\Delta r, m_M)$. Conversely, in Equation (9) $m_0 \in [m_{th}, m_M)$ and if $dM \to 0$, since $p(m|m_0)$ is an exponential decreasing function of m, the integral in Equation (9) is mainly controlled by the contribution from $m \simeq m_{th}$ which leads to $\rho_f(\Delta r, m_M) \simeq G(\Delta r, m_{th})$. As a consequence, in the ETAS model, we expect that $\rho_f(\Delta r, m_M)$ only weakly depends on m_M differently from ρ_a. The comparison between Equations (8) and (9) therefore shows that independently of the value of the model parameters, the condition $\rho_a(\Delta r, m_M) \simeq \rho_f(\Delta r, m_M)$ cannot be reproduced by the ETAS model. This is confirmed by Figure 4 where the symmetrical behavior $\zeta_a(\Delta r, m_M) \simeq \zeta_f(\Delta r, m_M)$, observed in the instrumental catalogs, is not recovered in the ETAS catalogs. Equations (8) and (9) also indicate that $\rho_a(\Delta r, m_M)$ is substantially independent of the value of m_{th} whereas $\rho_f(\Delta r, m_M)$ is expected to significantly depend on it, in agreement with numerical simulations of the ETAS model [29]. In instrumental catalogs, conversely, the symmetry $\rho_a(\Delta r, m_M) \simeq \rho_f(\Delta r, m_M)$ is observed quite independently of the value

of m_{th} [29]. This is another important difference of the spatial distribution of foreshocks between instrumental and ETAS catalogs.

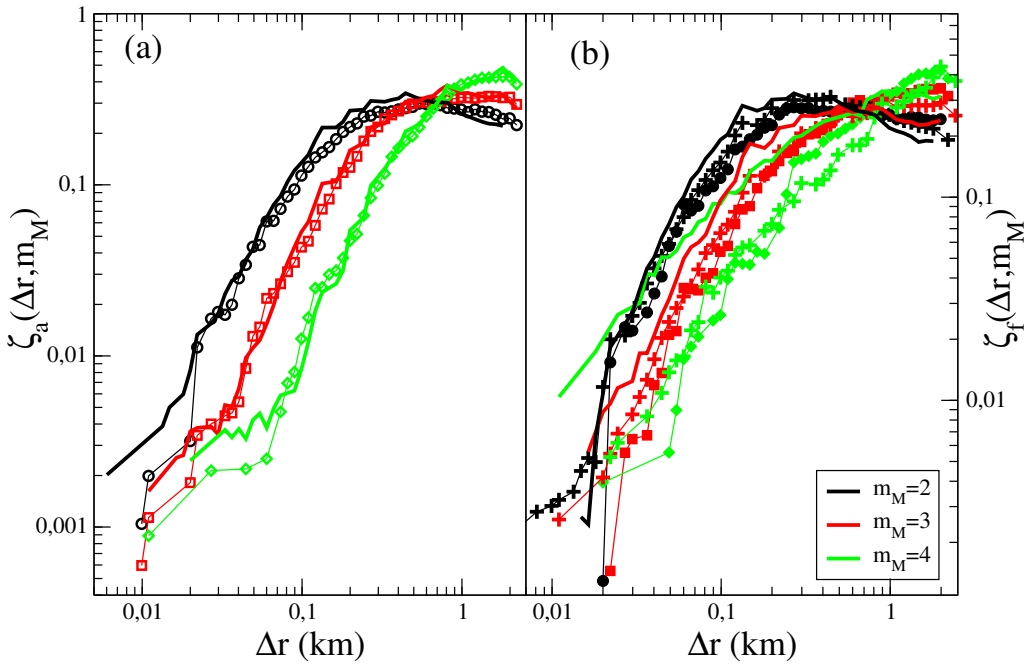

Figure 4. (Color online) (Left panel) The average distance of aftershocks $\zeta_a(\Delta r, m_M)$ in the RSCEC (open symbols) and in the synthetic ETASI2 catalogs (continuous lines) is plotted as function of Δr for different mainshock magnitude classes. (Right Panel) The average distance of foreshocks $\zeta_f(\Delta r, m_M)$ in the RSCEC (filled symbols) and in the synthetic ETASI2 catalog (continuous lines) is plotted as function of Δr for different mainshock magnitude classes. Results for the EATFS model, for the best set of model parameters listed in Table 1, are plotted with crosses.

4.3. Results in the ETASI2 Catalog

Results of the previous section show that ETAS catalogs contain fewer aftershocks than instrumental catalogs. A possible explanation of the foreshock deficit is related to the difficulty to identify small events which occur soon after larger ones as discussed in Section 2.2. This makes instrumental catalog incomplete in the first part of the aftershock sequence. As a consequence, the value of A, implemented in the ETAS model to recover the instrumental ratio $n_{aft}(m_M)/n_{main}(m_M)$, is underestimated as well as the ratio of $n_{fore}(m_M)/n_{main}(m_M)$. In this section we take explicitly into account the role of incompleteness by studying aftershocks and foreshocks statistical feature in the ETASI2 catalog.

We have performed extended numerical simulations of the ETASI2 model exploring a wide range of model parameters and evaluated $n_{aft}(m_M)$ and $n_{fore}(m_M)$. Restricting to parameters with $n_{aft}(m_M)/n_{main}(m_M)$ in agreement with the instrumental RSCEC catalog, we find (Figure 3) that, as expected, the incompleteness increases the value of $n_{fore}(m_M)/n_{aft}(m_M)$ which, however, still remains systematically smaller than the value found in instrumental catalogs. For fixed ψ and Δm in Equation (3), the ratio $n_{fore}(m_M)/n_{aft}(m_M)$ does not strongly depend on different choices of σ, as well as on different values of A, p, c and it is always significant smaller than the instrumental one. We also find that $n_{fore}(m_M)/n_{aft}(m_M)$ slightly increases for decreasing Δm and becomes approximately Δm independent for $\Delta m \lesssim 0$. However, also in this case the value $n_{fore}(m_M)/n_{aft}(m_M)$ is significantly smaller than the one measured in the instrumental catalogs. The origin of this discrepancy is that incompleteness also affects the foreshock number. Indeed, considering a mainshock of magnitude m_2 anticipated by an event (a foreshock) with magnitude $m_1 < m_2$, incompleteness does not only affect the identification of both m_1 and m_2 but it can hide foreshocks with magnitude $m < m_1$ occurring between

them. Therefore, if the parameters are tuned in order to produce a higher aftershock incompleteness this also reduces the foreshock number and the experimental result is never recovered. In Figure 1 we plot for each instrumental catalog the results of the ETASI2 model for parameters leading to the best agreement for $n_{aft}(m_M)/n_{main}(m_M)$ and minimizing the discrepancy for $n_{fore}(m_M)/n_{main}(m_M)$. Results are obtained assuming $\phi = 0.75$ and $\Delta m = 0.8$ for all catalogs, and keeping $\sigma = 0.3$. Furthermore we use $p = 1.2$ and $c = 0.01$ s. The values of A and α producing the best agreement are listed in the caption of Figure 1.

In numerical simulations (not shown) of the ETASI model we find that the spatial distribution of aftershocks in the ETASI2 and in the ETAS model are practically indistinguishable. Indeed, incompleteness typically affects the number of aftershocks but not their spatial distributions. The same observation also holds for the spatial distribution of foreshocks. Therefore, as in the ETAS model, the same deviations from the instrumental finding $\zeta_a(\Delta r, m_M) \simeq \zeta_f(\Delta r, m_M)$ is also observed in ETASI2 catalogs.

4.4. Results in ETAFS Catalogs

Previous section have shown a systematic deficit of foreshocks in ETAS catalogs which cannot be attributed to the incompleteness of the instrumental catalogs. This motivates the addition of events, different from the ones already implemented in the ETAS catalogs, as in the ETAFS model (Section 2.3). In numerical simulations of the ETAFS model we fix $c = 100$ s and chose the parameters B, c', α', for each instrumental catalog, in order to reproduce the value $n_{fore}(m_M)/n_{main}(m_M)$, for different m_M (see Table 1). We also take explicitly into account aftershock incompleteness, implemented as in the ETASI2 model, and finally generate synthetic catalogs with the same value of $n_{aft}(m_M)/n_{main}(m_M)$ and $n_{fore}(m_M)/n_{main}(m_M)$ as instrumental ones. Figure 3 shows that for all values of m_M ETAFS catalogs contains the same number of both aftershocks and foreshocks of instrumental data sets.

Interestingly, adding the "extra" foreshocks allows us to generate numerical catalogs which reproduce also the result $\zeta_a(\Delta r, m_M) \simeq \zeta_f(\Delta r, m_M)$, observed in instrumental catalogs (Figure 2). Indeed, in (Figure 4) we compare the average fore-mainshock distance $\zeta_f(\Delta r, m_M)$ between the ETAFS and the RSCEC catalog and obtain satisfactory agreement for all values of m_M.

Table 1. Best parameters of the ETAFS model.

Catalog	A	α	B	α_f	μ s^{-1}
RSCEC	0.084	0.9	0.050	0.54	5.84×10^{-4}
RNCEC	0.082	0.88	0.033	0.59	4.98×10^{-4}
ItEC	0.086	0.88	0.052	0.60	5.21×10^{-4}
JapEC	0.234	0.6	0.160	0.36	5.92×10^{-3}

5. Conclusions

We have shown that in four different instrumental regional catalogs, the configuration where a smaller earthquake precedes the occurrence of a larger one occurs more frequently than what expected according to the ETAS model. Furthermore, the average spatial distance between the two earthquakes in instrumental catalogs is significantly larger than predicted by the ETAS model. These results support the idea that the preparatory phase of an earthquake can be accompanied by the nucleation of small earthquakes, a mechanism expected according to the nucleation theory [13–15] but not present in the ETAS model. We have therefore presented a novel model which, together with the usual aftershock triggering, assumes that an earthquake can be anticipated by the occurrence of smaller ones. The occurrence probability of these small events is formalized on the basis of statistical empirical features of foreshocks without any a priori physical explanation. The model is supported by its efficiency in reproducing statistical features of both aftershocks and foreshocks in instrumental catalogs.

All properties investigated in this study are obtained by means of a stacking procedure. An interesting point is the behavior expected according to the ETAFS model for the seismic activity before a single large shock. The best-fit parameters of the ETAFS model (Table 1) indicate a small coefficient $\alpha_f \simeq 0.5$ in the foreshock productivity law and accordingly the number of foreshock remains relatively small also before large m_M. For instance, we expect on average less than 8 ($m > 2$) foreshocks the day before a magnitude $m = 7$ mainshock, within a radius of 10 km. This small number implies that for a single mainshock, foreshock activity can at most appear in the form of isolated bursts not leading to an evident systematic increase of the seismic rate. This is consistent with experimental observations, where the inverse Omori-law is obtained only after a stacking procedure and rarely observed inside isolated sequences [59,60].

The agreement with experimental data suggests that the ETAFS model can contribute to a significant improvement of pre-seismic forecasting. A rigorous validation of this point, however, needs to be tested in prospective tests. Unfortunately, a main limitation of the model is that it is not immediately suitable to be implemented in this kind of analysis. Indeed, in order to forecast the occurrence of an earthquake, according to the ETAFS model it is necessary to distinguish foreshock from normal earthquake triggering. An attempt in this direction can be found in [17] where the ETAS occurrence probability is multiplied by an ad-hoc function which gives different weights to aftershock and foreshock clustering. This produces significant gain in the retrospective forecasting of $m > 6$ earthquakes. The nature of foreshocks implemented in the ETAFS model is consistent with this approach promoting further studies on the relevance of foreshocks in seismic forecasting.

Author Contributions: All authors contributed equally to the conceptualization, the formal analysis and the writing of this manuscript.

Funding: This research received no external funding.

Acknowledgments: We thank the National Research Institute for Earth Science and Disaster Prevention for the mainland Japan catalog.

Conflicts of Interest: The authors declare no conflict of interest.

References

1. Ogata, Y. Statistical Models for Earthquake Occurrences and Residual Analysis for Point Processes. *J. Am. Stat. Assoc.* **1988**, *83*, 9–27. [CrossRef]
2. Ogata, Y. Space-time Point-process Models for Earthquake Occurrences. *Ann. Inst. Stat. Math.* **1988**, *50*, 379–402. [CrossRef]
3. Ogata, Y. A Monte Carlo method for high dimensional integration. *Numer. Math.* **1989**, *55*, 137–157. [CrossRef]
4. Huang, Q.; Gerstenberger, M.; Zhuang, J. Current Challenges in Statistical Seismology. *Pure Appl. Geophys.* **2016**, *173*, 1–3. [CrossRef]
5. Corral, A. Long-Term Clustering, Scaling, and Universality in the Temporal Occurrence of Earthquakes. *Phys. Rev. Lett.* **2004**, *92*, 108501. [CrossRef] [PubMed]
6. Corral, A. Renormalization-Group Transformations and Correlations of Seismicity. *Phys. Rev. Lett.* **2005**, *95*, 028501. [CrossRef] [PubMed]
7. Corral, A. Scaling and universality in the dynamics of seismic occurrence and beyond. In *Acoustic Emission and Critical Phenomena*; CRC Press: Boca Raton, FL, USA, 2008; pp. 225–244.
8. Bottiglieri, M.; de Arcangelis, L.; Godano, C.; Lippiello, E. Multiple-Time Scaling and Universal Behavior of the Earthquake Interevent Time Distribution. *Phys. Rev. Lett.* **2010**, *104*, 158501. [CrossRef] [PubMed]
9. Lippiello, E.; Corral, A.; Bottiglieri, M.; Godano, C.; de Arcangelis, L. Scaling behavior of the earthquake intertime distribution: Influence of large shocks and time scales in the Omori law. *Phys. Rev. E* **2012**, *86*, 066119. [CrossRef] [PubMed]
10. Varotsos, P.A.; Sarlis, N.V.; Skordas, E.S.; Tanaka, H.K.; Lazaridou, M.S. Attempt to distinguish long-range temporal correlations from the statistics of the increments by natural time analysis. *Phys. Rev. E* **2006**, *74*, 021123. [CrossRef]

11. Sarlis, N.V.; Skordas, E.S.; Varotsos, P.A. Nonextensivity and natural time: The case of seismicity. *Phys. Rev. E* **2010**, *82*, 021110. [CrossRef]
12. de Arcangelis, L.; Godano, C.; Grasso, J.R.; Lippiello, E. Statistical physics approach to earthquake occurrence and forecasting. *Phys. Rep.* **2016**, *628*, 1–91. [CrossRef]
13. Ohnaka, M. Earthquake source nucleation: A physical model for short-term precursors. *Tectonophysics* **1992**, *211*, 149–178. [CrossRef]
14. Ohnaka, M. Critical Size of the Nucleation Zone of Earthquake Rupture Inferred from Immediate Foreshock Activity. *J. Phys. Earth* **1993**, *41*, 45–56. [CrossRef]
15. Dodge, D.A.; Beroza, G.C.; Ellsworth, W.L. Detailed observations of California foreshock sequences: Implications for the earthquake initiation process. *J. Geophys. Res. Solid Earth* **1996**, *101*, 22371–22392. [CrossRef]
16. Brodsky, E.E. The spatial density of foreshocks. *Geophys. Res. Lett.* **2011**, *38*, L10305. [CrossRef]
17. Lippiello, E.; Marzocchi, W.; de Arcangelis, L.; Godano, C. Spatial organization of foreshocks as a tool to forecast large earthquakes. *Sci. Rep.* **2012**, *2*, 846. [CrossRef] [PubMed]
18. Shearer, P.M. Self-similar earthquake triggering, Bath's law, and foreshock/aftershock magnitudes: Simulations, theory, and results for Southern California. *J. Geophys. Res.-Solid Earth* **2012**, *117*. [CrossRef]
19. Shearer, P.M. Space-time clustering of seismicity in California and the distance dependence of earthquake triggering. *J. Geophys. Res. Solid Earth* **2012**, *117*. [CrossRef]
20. Hainzl, S. Comment on "Self-similar earthquake triggering, Båth's law, and foreshock/aftershock magnitudes: Simulations, theory, and results for southern California" by P. M. Shearer. *J. Geophys. Res. Solid Earth* **2013**, *118*, 1188–1191. [CrossRef]
21. Shearer, P.M. Reply to comment by S. Hainzl on "Self-similar earthquake triggering, Båth's Law, and foreshock/aftershock magnitudes: Simulations, theory and results for southern California". *J. Geophys. Res. Solid Earth* **2013**, *118*, 1192. [CrossRef]
22. Bouchon, M.; Durand, V.; Marsan, D.; Karabulut, H.; Schmittbuhl, J. The long precursory phase of most large interplate earthquakes. *Nat. Geosci.* **2013**, *6*, 299–302. [CrossRef]
23. Mignan, A. The debate on the prognostic value of earthquake foreshocks: A meta-analysis. *Sci. Rep.* **2014**, *4*, 4099–4103. [CrossRef] [PubMed]
24. Chen, X.W.; Shearer, P.M. California foreshock sequences suggest aseismic triggering process. *Geophys. Res. Lett.* **2013**, *40*, 2602–2607. [CrossRef]
25. Brodsky, E.E.; Lay, T. Recognizing Foreshocks from the 1 April 2014 Chile Earthquake. *Science* **2014**, *344*, 700–702. [CrossRef]
26. Ogata, Y.; Katsura, K. Comparing foreshock characteristics and foreshock forecasting in observed and simulated earthquake catalogs. *J. Geophys. Res. Solid Earth* **2014**, *119*, 8457–8477. [CrossRef]
27. Felzer, K.R.; Page, M.T.; Michael, A.J. Artificial seismic acceleration. *Nat. Geosci.* **2015**, *8*, 82–83. [CrossRef]
28. Bouchon, M.; Marsan, D. Reply to 'Artificial seismic acceleration'. *Nat. Geosci.* **2015**, *8*, 83. [CrossRef]
29. Lippiello, E.; Giacco, F.; Marzocchi, W.; Godano, C.; Arcangelis, L.D. Statistical Features of Foreshocks in Instrumental and ETAS Catalogs. *Pure Appl. Geophys.* **2017**, 1–19. [CrossRef]
30. Seif, S.; Zechar, J.D.; Mignan, A.; Nandan, S.; Wiemer, S. Foreshocks and Their Potential Deviation from General SeismicityForeshocks and Their Potential Deviation from General Seismicity. *Bull. Seismol. Soc. Am.* **2018**, *109*. [CrossRef]
31. Kagan, Y.Y. Short-Term Properties of Earthquake Catalogs and Models of Earthquake Source. *Bull. Seismol. Soc. Am.* **2004**, *94*, 1207–1228. [CrossRef]
32. Helmstetter, A.; Kagan, Y.Y.; Jackson, D.D. Comparison of Short-Term and Time-Independent Earthquake Forecast Models for Southern California. *Bull. Seismol. Soc. Am.* **2006**, *96*, 90–106. [CrossRef]
33. Enescu, B.; Mori, J.; Miyazawa, M. Quantifying early aftershock activity of the 2004 mid-Niigata Prefecture earthquake (Mw6.6). *J. Geophys. Res. Solid Earth* **2007**, *112*, B04310. [CrossRef]
34. Peng, Z.; Vidale, J.E.; Ishii, M.; Helmstetter, A. Seismicity rate immediately before and after main shock rupture from high-frequency waveforms in Japan. *J. Geophys. Res. Solid Earth* **2007**, *112*, B03306. [CrossRef]
35. Peng, Z.; Zhao, P. Migration of early aftershocks following the 2004 Parkfield earthquake. *Nat. Geosci.* **2009**, *2*, 877–881. [CrossRef]
36. Omi, T.; Ogata, Y.; Hirata, Y.; Aihara, K. Forecasting large aftershocks within one day after the main shock. *Sci. Rep.* **2013**, *3*, 2218. [CrossRef] [PubMed]

37. Lippiello, E.; Cirillo, A.; Godano, G.; Papadimitriou, E.; Karakostas, V. Real-time forecast of aftershocks from a single seismic station signal. *Geophys. Res. Lett.* **2016**, *43*, 6252–6258. [CrossRef]
38. Hainzl, S. Apparent triggering function of aftershocks resulting from rate-dependent incompleteness of earthquake catalogs. *J. Geophys. Res. Solid Earth* **2016**, *121*, 6499–6509. [CrossRef]
39. Hainzl, S. Rate-Dependent Incompleteness of Earthquake Catalogs. *Seismol. Res. Lett.* **2016**, *87*, 337–344. [CrossRef]
40. de Arcangelis, L.; Godano, C.; Lippiello, E. The overlap of aftershock coda-waves and short-term post seismic forecasting. *J. Geophys. Res. Solid Earth* **2018**, *123*, 5661–5674. [CrossRef]
41. Shcherbakov, R.; Yakovlev, G.; Turcotte, D.L.; Rundle, J.B. Model for the Distribution of Aftershock Interoccurrence Times. *Phys. Rev. Lett.* **2005**, *95*, 218501. [CrossRef]
42. Lippiello, E.; Bottiglieri, M.; Godano, C.; de Arcangelis, L. Dynamical scaling and generalized Omori law. *Geophys. Res. Lett.* **2007**, *34*, L23301. [CrossRef]
43. Bottiglieri, M.; de Arcangelis, L.; Godano, C.; Lippiello, E. The Generalized Omori law: Magnitude incompleteness or magnitude clustering. *Int. J. Mod. Phys. B* **2009**, *23*, 5597–5608. [CrossRef]
44. Bottiglieri, M.; Lippiello, E.; Godano, C.; de Arcangelis, L. Identification and spatiotemporal organization of aftershocks. *J. Geophys. Res. Solid Earth* **2009**, *114*, B03303. [CrossRef]
45. Bottiglieri, M.; Lippiello, E.; Godano, C.; de Arcangelis, L. Comparison of branching models for seismicity and likelihood maximization through simulated annealing. *J. Geophys. Res. Solid Earth* **2011**, *116*, B02303. doi:10.1029/2009JB007060. [CrossRef]
46. Davidsen, J.; Baiesi, M. Self-similar aftershock rates. *Phys. Rev. E* **2016**, *94*, 022314. [CrossRef] [PubMed]
47. Lippiello, E.; Godano, C.; de Arcangelis, L. Dynamical Scaling in Branching Models for Seismicity. *Phys. Rev. Lett.* **2007**, *98*, 098501. [CrossRef] [PubMed]
48. Lippiello, E.; de Arcangelis, L.; Godano, C. Influence of Time and Space Correlations on Earthquake Magnitude. *Phys. Rev. Lett.* **2008**, *100*, 038501. [CrossRef]
49. Lippiello, E.; de Arcangelis, L.; Godano, C. Time, Space and Magnitude Correlations in Earthquake Occurrence. *Int. J. Mod. Phys. B* **2009**, *23*, 5583–5596. [CrossRef]
50. Lippiello, E.; de Arcangelis, L.; Godano, C. Role of Static Stress Diffusion in the Spatiotemporal Organization of Aftershocks. *Phys. Rev. Lett.* **2009**, *103*, 038501. [CrossRef]
51. Sarlis, N.V. Magnitude correlations in global seismicity. *Phys. Rev. E* **2011**, *84*, 022101. [CrossRef]
52. Lippiello, E.; Godano, C.; de Arcangelis, L. The earthquake magnitude is influenced by previous seismicity. *Geophys. Res. Lett.* **2012**, *39*, L05309. [CrossRef]
53. Lippiello, E.; Godano, C.; de Arcangelis, L. Magnitude correlations in the Olami-Feder-Christensen model. *Europhys. Lett.* **2013**, *102*, 59002. [CrossRef]
54. Hauksson, E.; Shearer, P.; Yang, W. Waveform relocated earthquake catalog for Southern California (1981 to June 2011). *Bull. Seismol. Soc. Am.* **2012**, *102*, 2239–2244. [CrossRef]
55. Waldhauser, F.; Schaff, D.P. Large-scale relocation of two decades of Northern California seismicity using cross-correlation and double-difference methods. *J. Geophys. Res. Solid Earth* **2008**, *113*, B08311. [CrossRef]
56. I.S.I.D.E. Italian Seismological Instrumental and Parametric Data-Base. Available online: http://cnt.rm.ingv.it/en/iside (accessed on 11 February 2019).
57. From Japan Meteorological Agency Earthquake Catalog, provided by N.I.E.D. Available online: https://wwweic.eri.u-tokyo.ac.jp/db/jma/index.html (accessed on 11 February 2019).
58. Felzer, K.R.; Brodsky, E.E. Decay of aftershock density with distance indicates triggering by dynamic stress. *Nature* **2006**, *441*, 735–738. [CrossRef] [PubMed]
59. Papadopoulos, G.A.; Charalampakis, M.; Fokaefs, A.; Minadakis, G. Strong foreshock signal preceding the L'Aquila (Italy) earthquake (M_w 6.3) of 6 April 2009. *Nat. Hazards Earth Syst. Sci.* **2010**, *10*, 19–24. [CrossRef]
60. Daskalaki, E.; Spiliotis, K.; Siettos, C.; Minadakis, G.; Papadopoulos, G.A. Foreshocks and Short-Term Hazard Assessment to Large Earthquakes using Complex Networks: the Case of the 2009 L'Aquila Earthquake. *Nonlinear Process. Geophys. Discuss.* **2016**, *2016*, 1–20. [CrossRef]